Differencing between quiescent and flaring states of blazars using threshold autoregressive models

Klaudia Kowalczyk
Mentor: Dr Mariusz Tarnopolski

NICOLAUS COPERNICUS UNIVERSITY IN TORUŃ

Faculty of Physics, Astronomy and Informatics

June 6, 2024

Motivation

▶ The variability in blazars' light curves and power spectral densities have been studied extensively over the years in all energy bands.

▶ A wide range of methods and stochastic models were applied with the intention of improving the understanding of their variability.

▶ Methods used for differentiating flaring and quiescent states in blazar light curves are often arbitrary.

A more systematic approach is needed for uniformity among achieved results, e.g., modeling blazars' spectral energy distribution (SED), which can lead to constraining the physical mechanism governing the observed variability, in particular, the powerful flares.
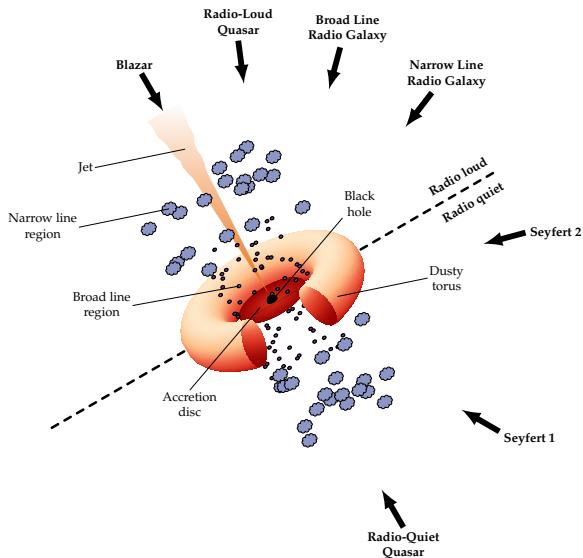
Active galactic nuclei

Figure 1: Unified model of AGN adapted from Urry and Padovani (1995). Created using LaTeX (PGFplots/TikZ).

Blazars

▶ Blazars are a unique class of active galactic nuclei (AGNs) hosting relativistic jets that point almost directly at the observer.

▶ They are observed in the whole electromagnetic spectrum, from radio waves to very high energy gamma-ray photons.

▶ They are known to be highly variable sources in all energy bands, particularly in gamma rays, in which they exhibit powerful flares.
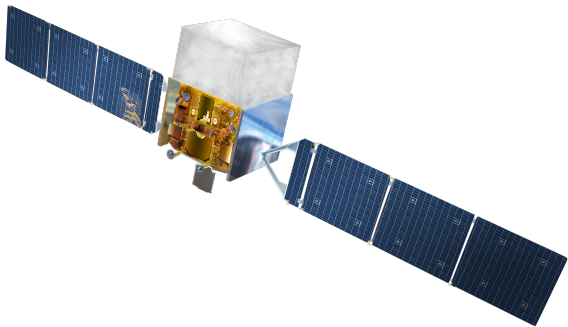
Fermi

Figure 2: Fermi Gamma-ray Space Telescope, formerly Gamma-ray Large Area Space Telescope (GLAST). Credits: NASA (https://science.nasa.gov/get-involved/toolkits/spacecraft-icons).

- ▶ Fermi was launched June 11, 2008.
- ▶ Fermi carries two instruments:
    - ▶ the Large Area Telescope (LAT),
    - ▶ the Gamma-ray Burst Monitor (GBM).
- ▶ Fermi LAT has a large FoV, over 2 steradians (1/5 of the entire sky).
- ▶ It covers the entire sky every three hours.
- ▶ The telescope operates in the photon energy range of 8 keV to ∼300 GeV.

Gamma-ray emission from blazars
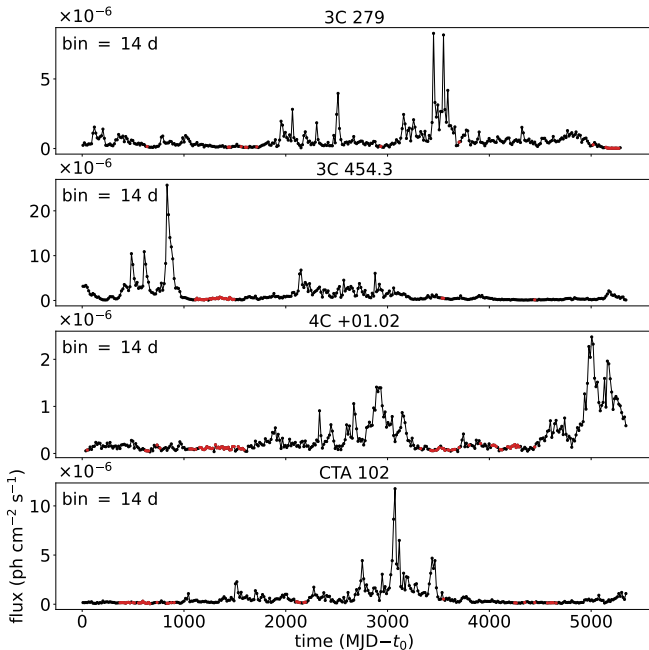
Data Sample

Forty-one blazars, some of the brightest from the 4FGL-DR4 catalog and the ones extensively discussed in the literature, were selected. The selected sources were divided into three groups

- the Gold Sample for at least 60% of data points having $TS > 25$ for all of the three bin sizes, counting 22 sources;
- the Silver Sample for at least 50% of data points having $TS > 25$ for at least one of the three bin sizes, counting 15 sources;
- the Brown Sample for at least 50% of data points having $TS > 25$ for all of the three bin sizes but with less than half of the original time range covered, counting 4 sources.
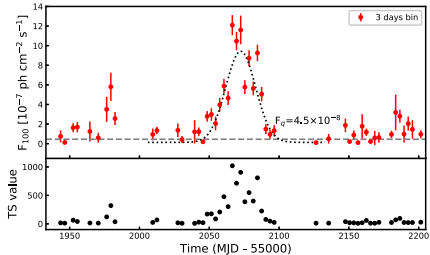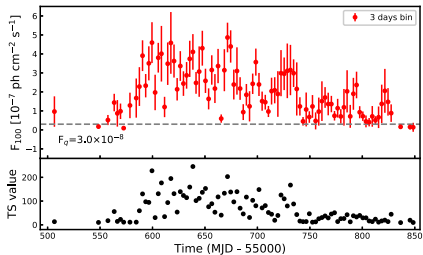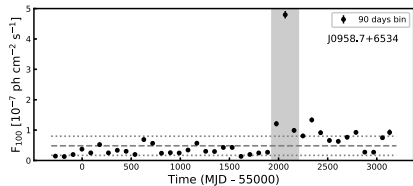
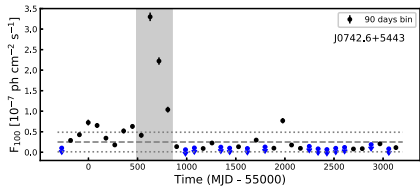# Quiescent and flaring states

Figure 4: Credits: Wang et al. (2020).

Autocorrelation function

▶ The non-parametric autocorrelation function (ACF) gives the correlation between a series and time-lagged values of itself over its entire length.

▶ For an evenly-spaced time series x:

$$ACF(k) = \frac{E[(x_t - \mu)(x_{t-k} - \mu)]}{\sigma^2}, \tag{1}$$

where μ is mean value and σ is standard deviation.

▶ In realistic cases, the population mean and standard deviation are unknown and must be estimated from the data.

▶ When the ACF shows significant signals, current values of the time series depend on past values. The time series violates the assumption of "independence" and many standard statistical procedures can not be accurately applied. This is the situation where autoregressive modelling can be effective.

Autoregressive modelling

AR

An autoregressive (AR) process has coefficients that quantify the dependence of current values on recent past values:

$$x_t = \varphi_1 x_{t-1} + \varphi_2 x_{t-2} + \cdots + \varphi_p x_{t-p} + \varepsilon_t, \quad (2)$$

where ε_t is a normally distributed random error with zero mean and constant variance, p is the order of the process, and φ_i are the corresponding coefficients for each lag.

MA

A moving average (MA) process has coefficients that quantify the dependence of current values on recent past random shocks to the system:

$$x_t = \epsilon_t + \theta_1 \varepsilon_{t-1} + \theta_2 \varepsilon_{t-2} + \cdots + \theta_q \varepsilon_{t-q}, \quad (3)$$

where ε_t is the error term for the t-th time point, q is the order of the process, and θ_i are the coefficients for each lagged error term.

ARMA

Adding the two equations together gives a combined ARMA(p,q) process:

$$x_t = c + \sum_{k=1}^{p} \varphi_k x_{t-k} + \sum_{l=1}^{q} \theta_l \varepsilon_{t-l} + \varepsilon_t, \quad (4)$$

where c is a constant. Coefficients are estimated by standard regression procedures such as maximum likelihood estimation.

MIARMA

- ▶ MIARMA is the gap-filling algorithm based on ARMA models written in MATLAB (Pascual-Granado, Garrido, et al., 2015; Pascual-Granado, Suárez, et al., 2018).
- ▶ MIARMA uses a forward-backward predictor based on autoregressive moving-average modeling (ARMA) in the time domain.
- ▶ The algorithm is particularly suitable for replacing invalid data such as those present in the light curves of space satellites (e.g. CoRoT, Kepler, TESS, PLATO, etc.) caused by instrumental effects, transit removal, or the impact of charged particles.
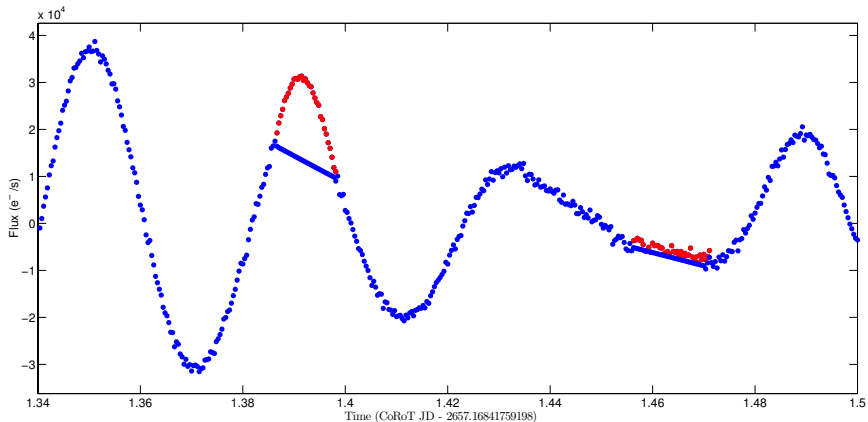
Figure 5: Comparison between ARMA gap-filling (red) and the linear interpolation (blue) for two gaps in the light curve of a δ Scuti star. Source: Pascual-Granado, Garrido, et al. (2015).

Threshold models

The basic family of ARMA models gives birth to many generalisations. One such generalisation accounts for regime-switching behaviour:

$$X_t = X_t^{(1)} I_{t-d} + X_t^{(2)} (1 - I_{t-d}) \tag{5}$$

i.e., when the dynamics of the process X_t change from $X_t^{(1)}$ to $X_t^{(2)}$, being two different ARMA processes, once the time series values cross a threshold r which is a free parameter to be determined by fitting to data. I_{t-d} is an indicator function which delay d, i.e. equal to 1 if $X_{t-d} \geq r$, and 0 if $X_{t-d} < r$.

Such models constitute a promising opportunity as they can provide means to distinguish quiescent states from flares in blazar light curves.

SETAR

▶ The self-exciting threshold autoregressive (SETAR) model, first presented by Tong (1983), can be considered as a direct generalization, in the non-linear domain, of the ARMA model (Box and Jenkins, 1976).

A SETAR model is defined as:

$$X_t = \left(\phi_0^{(1)} + \sum_{j=1}^{m_L} \phi_j^{(1)} X_{t-j} \right) I(z_t \leqslant \text{th})$$
$$+ \left(\phi_0^{(2)} + \sum_{k=1}^{m_H} \phi_k^{(2)} X_{t-k} \right) I(z_t > \text{th}) + \varepsilon_t,$$

where m_L and m_H are lower and higher orders of the model, I is an indicator function, and z_t is the threshold variable. An indicator function is equal to 1 if the threshold variable fulfills a set condition and is equal to 0 otherwise. The autoregressive expression correlates the current value of the series with a finite number of previous values.

Information Criteria

Best fit parameters for AMRA-type coefficients are typically calculated with maximum likelihood estimation for different values of p, d and q, called the order of the model. The optimal order is then selected to optimize the Information Criteria (e.g., AIC, BIC), a penalized maximum likelihood measure that balances improvements in likelihood with increases in model complexity.

Information Criteria

AIC

Akaike's Information Criteria:

$$AIC = -2\ln(L) + 2k, \qquad (6)$$

where L is the value of the likelihood and k is the number of estimated parameters.

BIC

Bayesian Information Criteria:

$$BIC = -2\ln(L) + 2\ln(N)k, \qquad (7)$$

where N is the number of recorded measurements.

- ▶ AIC and BIC reward goodness of fit (as assessed by the likelihood function), but they also include a penalty that is an increasing function of the number of estimated parameters. The penalty discourages overfitting, which is desired because increasing the number of parameters in the model almost always improves the goodness of the fit.

- ▶ The difference between the BIC and the AIC is the greater penalty imposed for the number of parameters by the former than the latter.
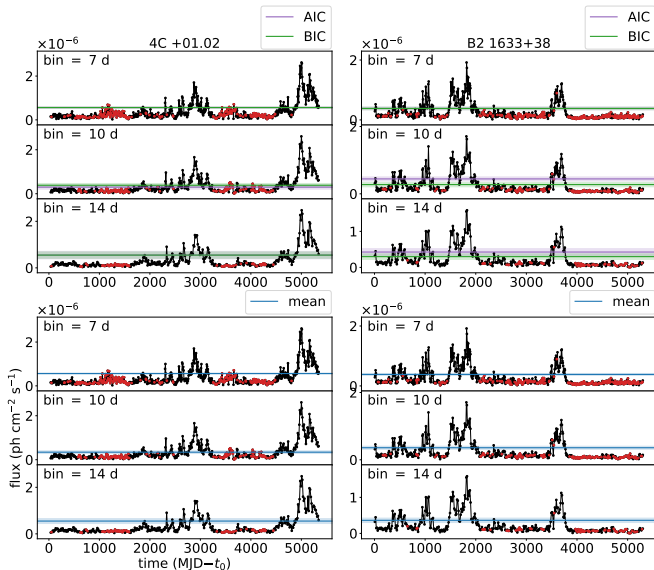
Quiescent vs flaring states

Figure 6: Example of light curves from the Fermi Gamma-ray Space Telescope. Red points indicate gaps interpolated with MIARMA.
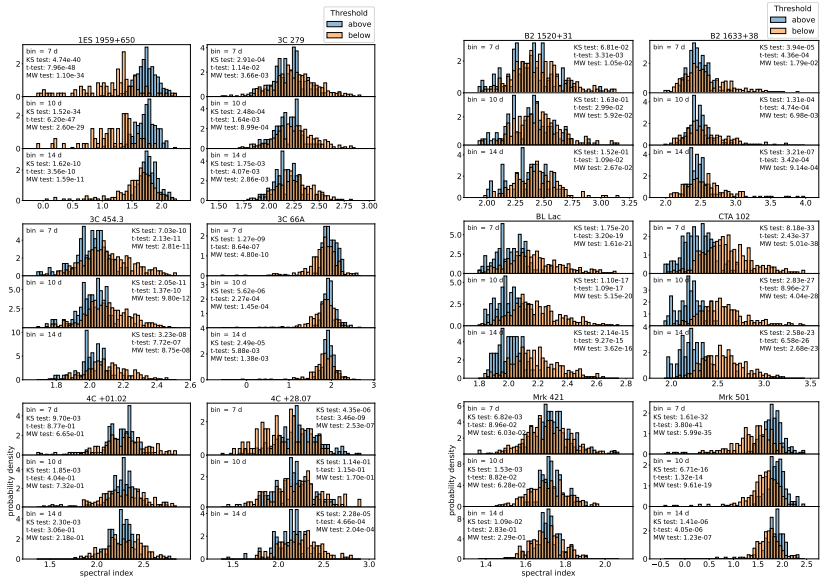
Spectral indices

Figure 7: Distribution of spectral index values depending on the corresponding flux being above or below the mean threshold estimate for the Gold Sample.

Flares duration

To determine flare duration, the time profile of a single flare (Abdo et al., 2010) was used in the following form

$$F(t) = F_c + F_0 \left(\exp\left(\frac{t_0 - t}{T_r} \right) + \exp\left(\frac{t - t_0}{T_d} \right) \right)^{-1}, \tag{8}$$

where F_c is the value of an assumed constant baseline underlying a flare, F_0 is the amplitude of a flare, t_0 represents the approximate time of the flare's peak, T_r measures the rise time, and T_d is the decay time. Then, the total duration of a flare can be estimated

$$T_{fl} \approx 2(T_r + T_d). \tag{9}$$

The observed flare time duration was transformed to a rest frame of reference using the relation

$$T_{fl}^{\text{rest}} = \frac{T_{fl}}{1 + z}. \tag{10}$$
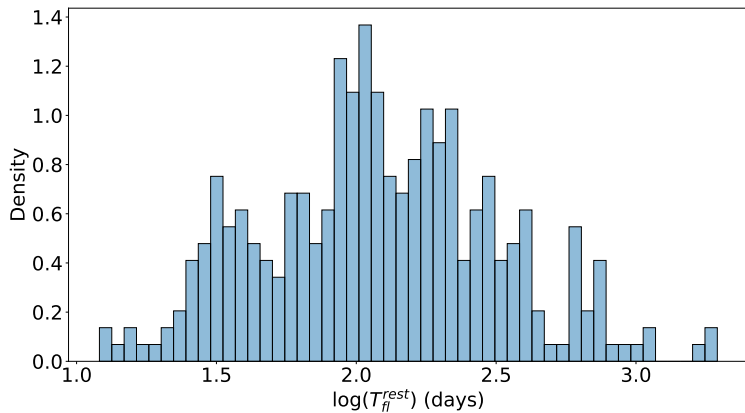
Flares duration

Figure 8: The distribution of flares duration times.

AGNs physical parameters

The variability characteristics were linked to the physical properties of AGNs adapted from Chen et al. (2023)

- ▶ the redshift z
- ▶ the black hole mass M
- ▶ the disc luminosity L_{disc} in units of erg s^{-1}
- ▶ the observed gamma-ray luminosity L_γ in units of erg s^{-1}
- ▶ the 1.4 GHz radio flux $f_{1.4\mathrm{GHz}}$ in units of Jy
- ▶ the jet kinetic power P_{jet} in units of erg s^{-1}
- ▶ the synchrotron peak frequency ν_{pk}^{sy}
- ▶ the Compton dominance CD
- ▶ the curvature b_{sy}
- ▶ the synchrotron peak frequency luminosity L_{pk}^{sy}

Definite correlations were found.

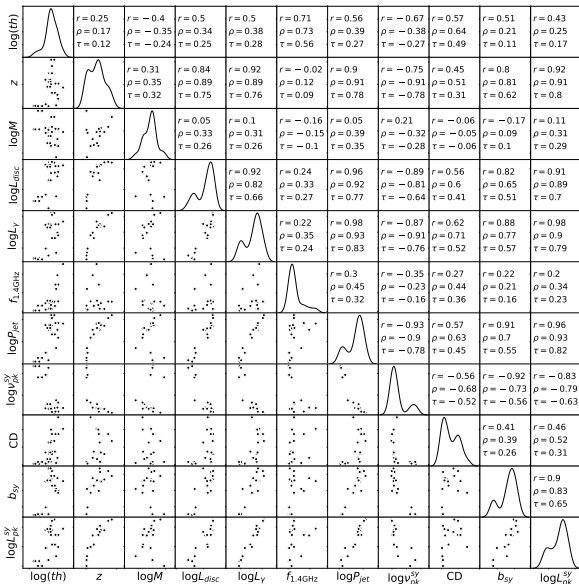# Threshold vs AGNs physical parameters

Figure 9: Correlations between the calculated threshold and other parameters taken from Chen et al. (2023).

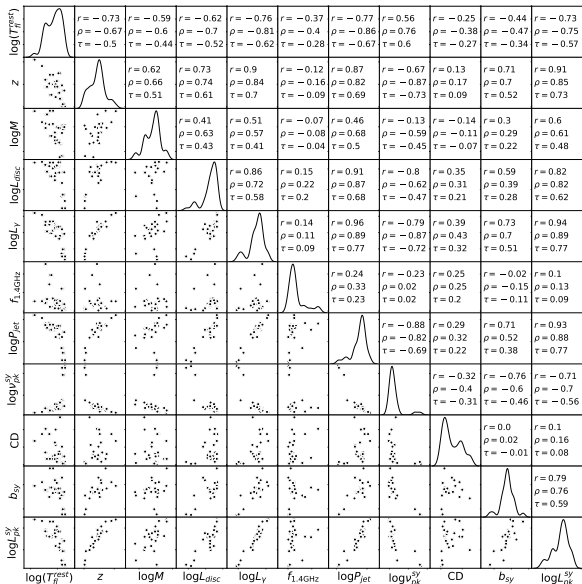# Flares duration vs AGNs physical parameters

Figure 10: Correlations between the determined flares duration and other parameters taken from Chen et al. (2023) with outliers removed.

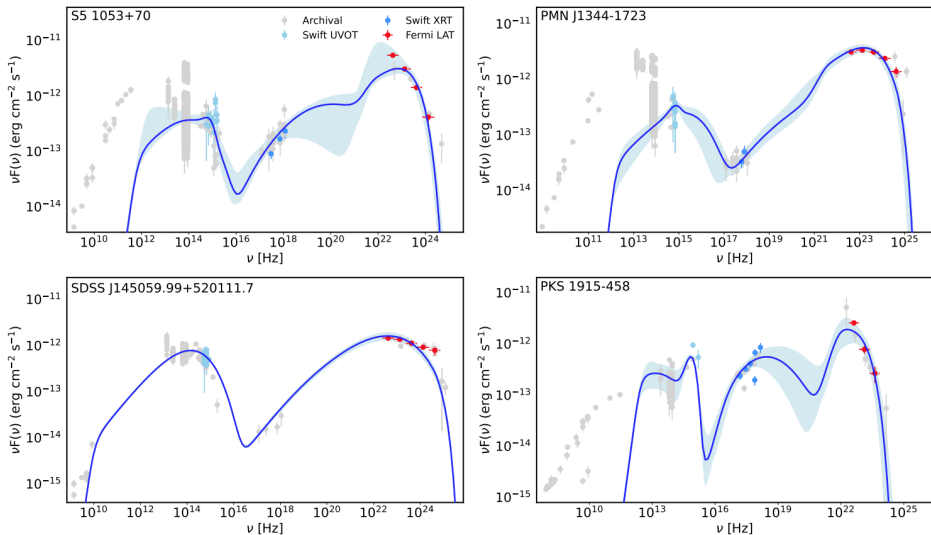# Next step: spectral energy distribution modeling

Figure 11: The broadband SED modeling results from Sahakyan et al. (2024).

Conclusions

▶ The SETAR model provides more objective and robust results in identifying flares in blazars' light curves than the often-used arbitrary methods.

▶ Locating flaring states is of importance when it comes to modeling the physical properties of blazars as it can provide valuable information on physical processes governing the variability, especially the activity during flares.

▶ Progress in the understanding of blazar variability may come from the study of a much larger sample of objects, focusing not only on the light curves but also a more detailed SED analysis, preferably the whole selection from the Fermi-LAT catalog, for a broader population analysis.

References

Abdo, A. A. et al. (2010). In: ApJ 722.1, p. 520.

Time series analysis. Forecasting and control (1976).

Chen, Y., Gu, Q., Fan, J., Yu, X., Ding, N., Xiong, D., and Guo, X. (2023). In: ApJ 944.2, 157, p. 157.

Pascual-Granado, J., Garrido, R., and Suárez, J. C. (2015). In: $A\&A$ 575, A78, A78.

Pascual-Granado, J., Suárez, J. C., Garrido, R., Moya, A., García Hernández, A., Rodón, J. R., and Lares-Martiz, M. (2018). In: $A\&A$ 614, A40, A40.

Sahakyan, N., Harutyunyan, G., Gasparyan, S., and Israyelyan, D. (2024). In: $MNRAS$ 528.4, pp. 5990–6009.

Tong, H. (1983). *Threshold Models in Non-linear Time Series Analysis*. Lecture notes in statistics. Springer-Verlag. URL: https://books.google.pl/books?id=J4lYAAAAYAAJ.

Urry, C. M. and Padovani, P. (1995). In: $PASP$ 107, p. 803.

Wang, G., Wang, Z., Chen, L., Zhou, J., and Xing, Y. (2020). In: $PASJ$ 72.1, 9, p. 9.